MCB
Journals.ASM.org

Analysis of Mice Lacking the Heparin-Binding Splice Isoform of Platelet-Derived Growth Factor A

Johanna Andrae,[a] Hans Ehrencrona,[b] Radiosa Gallini,[a,c] Mark Lal,[c]* Hao Ding,[d] Christer Betsholtz[a,c]

Department of Immunology, Genetics and Pathology, Uppsala University, Rudbeck Laboratory, Uppsala, Sweden[a]; Department of Clinical Genetics, Lund University Hospital, Lund, Sweden[b]; Department of Medical Biochemistry and Biophysics, Karolinska Institutet, Stockholm, Sweden[c]; Department of Biochemistry and Medical Genetics, University of Manitoba, Winnipeg, Manitoba, Canada[d]

Platelet-derived growth factor A-chain (PDGF-A) exists in two evolutionarily conserved isoforms, PDGF-A_{long} and PDGF-A_{short}, generated by alternative RNA splicing. They differ by the presence (in PDGF-A_{long}) or absence (in PDGF-A_{short}) of a carboxy-terminal heparin/heparan sulfate proteoglycan-binding motif. In mice, similar motifs present in other members of the PDGF and vascular endothelial growth factor (VEGF) families have been functionally analyzed *in vivo*, but the specific physiological importance of PDGF-A_{long} has not been explored previously. Here, we analyzed the absolute and relative expression of the two PDGF-A splice isoforms during early postnatal organ development in the mouse and report on the generation of a *Pdgfa* allele (*Pdgfa*$^{\Delta ex6}$) incapable of producing PDGF-A_{long} due to a deletion of the exon 6 splice acceptor site. In situations of limiting PDGF-A signaling through PDGF receptor alpha (PDGFRα), or in mice lacking PDGF-C, homozygous carriers of *Pdgfa*$^{\Delta ex6}$ showed abnormal development of the lung, intestine, and vertebral column, pinpointing developmental processes where PDGF-A_{long} may play a physiological role.

The development of multicellular organisms requires cell-cell interactions. Some of these depend on soluble paracrine ligands that are released from cells in order to bind to receptors on neighboring cells and thereby elicit local control of cell migration, proliferation, death, and differentiation. The outcome for the individual cell depends on the identity and local concentration of the signaling molecules, as well as their cognate receptors, as exemplified by morphogens of the Hedgehog, transforming growth factor beta (TGF-β), and Wnt families. The distribution of the active ligands in gradients or depots in the extracellular space is also important. For example, the distribution of vascular endothelial growth factor A (VEGF-A) in gradients is necessary for proper migration of so-called endothelial tip cells, which spearhead angiogenic sprouts, and for the formation of a correctly patterned and functional vasculature (1, 2). Growth factor gradients may be created through cell-type-specific and polarized protein secretion, by binding to the extracellular matrix (ECM), and through unequal distribution of ligand-modifying enzymes (reviewed in reference 3) Thus, numerous processes contribute to the control of the distribution and bioavailability of growth factors and other signaling molecules during embryonic development and other physiological and pathophysiological morphogenetic processes.

A number of extracellular signaling proteins, including growth factors, morphogens, cytokines, and enzymes (collectively referred to as ligands), possess an ability to bind to heparin and heparan sulfate proteoglycans (HSPGs). In several cases, this interaction has been mapped to specific molecular domains and shown to depend on stretches of positively charged (basic) amino acid residues present in the ligand and negatively charged groups present in heparin/HSPGs (reviewed in reference 4). A few basic amino acid residues seem to be sufficient to confer HSPG binding. For example, mutagenesis of bone morphogenetic protein 4 (BMP-4) in *Xenopus* has indicated that loss of three basic amino acid residues reduced ECM retention of BMP-4, resulting in developmental-patterning defects (5).

HSPGs are critical regulators of developmentally important signaling molecules, such as Wnts, Hedgehogs, TGF-β/BMPs, and fibroblast growth factors (FGFs) (reviewed in references 3, 6, and 7). Heparin-binding retention motifs are also present in several growth factors of the platelet-derived growth factor (PDGF)/VEGF family. Alternative splicing of the mRNAs for platelet-derived growth factor A-chain (PDGF-A), VEGF-A, VEGF-B, and placenta growth factor (PlGF) generates isoforms of the respective growth factor, which differ in their affinities for HSPGs and the ECM (reviewed in references 8, 9, and 10). In PDGF-B, the presence or absence of an HSPG-binding retention motif depends on alternative proteolytic processing of its C terminus (11, 12). The physiological importance of HSPG binding of VEGF/PDGF family members has been analyzed in mice by targeted mutagenesis that selectively eliminates different splice variants in VEGF-A (1, 2, 13) or deletes the retention motif in PDGF-B (14, 15). For VEGF-A, loss of the HSPG-binding splice isoforms results in abrogated angiogenic sprouting and the formation of abnormally few and wide blood vessels (1, 2). In PDGF-B, deletion of the retention motif results in impaired recruitment of pericytes to newly formed blood vessels (15). A similar phenotype was also observed in mice lacking *N*-deacetylase/*N*-sulfotransferase 1 (NSTD-1), an enzyme involved in the formation of heparan sulfate (4, 14). Thus, binding of VEGFs and PDGF-B to HSPGs appears to be critical during development. Evidence for a specific physiological role *in vivo* for the HSPG-binding isoform of PDGF-A has been lacking until now, however.

Received 13 June 2013 Returned for modification 9 July 2013
Accepted 5 August 2013
Published ahead of print 12 August 2013
Address correspondence to Christer Betsholtz, christer.betsholtz@igp.uu.se.
* Present address: Mark Lal, Astrazeneca AB, Mölndal, Sweden.

doi:10.1128/MCB.00749-13

In humans, the *PDGF-A* gene is located on chromosome 7 and contains seven exons (16, 17). Alternative splicing of the *PDGF-A* transcript generates two different isoforms of the protein—PDGF-A_{long} and PDGF-A_{short} (17, 18)—which differ at the C terminus. PDGF-A_{long} results from the inclusion of a separate exon (exon 6), which encodes a stretch of 18 C-terminal amino acid residues, 10 of which are basic. Instead, PDGF-A_{short} has three C-terminal amino acids encoded by exon 7, none of which are basic. *In vitro* studies have demonstrated that the ECM binds PDGF-A_{long}, leading to a high local concentration around the cells from which it is expressed, whereas PDGF-A_{short} is freely diffusible in the cell culture medium (19, 20). The two PDGF-A splice variants are conserved across vertebrate species, i.e., they have been demonstrated in human, mouse, rat, hamster, chick, frog, and pig (reviewed in references 21, 22, and 23). Both PDGF-A_{long} and PDGF-A_{short} can be found in normal cells, as well as in tumor cells (22), although some early reports claimed PDGF-A_{long} was tumor specific (24).

The exon 6-encoded retention motif binds to heparin and HSPGs, leading to its association with the ECM (20, 25). Three basic amino acid residues encoded by exon 6 are essential for HSPG interaction (25, 26), but it has also been suggested that the total positive charge of the retention sequence is more important than any specific amino acid residues (19). The heparin–PDGF-A interaction takes place via N-sulfated saccharide groups on the heparin/HSPGs (27). PDGF-A_{long} has 100 times higher affinity to heparin than PDGF-A_{short} (26). The presence of the retention motif has no dramatic effect on the binding specificity or affinity of PDGF-A for the PDGF receptors. Scatchard analysis demonstrated that PDGF-A_{long} has a 1.5-fold-lower affinity for PDGF receptor alpha (PDGFRα) than PDGF-A_{short}; however, neither PDGF-A_{long} nor PDGF-A_{short} binds PDGF receptor beta (PDGFRβ) with any significant affinity (28).

Some tissues (e.g., the central nervous system [CNS]) appear to express more alternatively spliced mRNAs than others. Alternative splicing is controlled by splicing factors, which regulate interaction between the spliceosome and splice sites. Splicing factors can be activated via phosphorylation/dephosphorylation, and their relative concentrations are important for splice site selection (reviewed in reference 29). Small changes in concentration and/or activity may alter the choice of splice site. A few cell-type-specific factors have been identified (e.g., epithelial splicing regulatory protein 1 [ESRP1]) that for some proteins regulate the choice of epithelial/mesenchymal-cell-specific splice isoforms (30). Tissue-specific gene expression signatures for splicing factors have also been identified as a way to control alternative splicing (31).

To assess the physiological role of PDGF-A_{long}, we generated mice homozygous for a targeted deletion of the splice acceptor site in exon 6 of the *Pdgfa* gene ($Pdgfa^{\Delta ex6/\Delta ex6}$). These mice lack the long *Pdgfa* mRNA and, consequently, the PDGF-A_{long} protein. Our analysis of these mice and compound mutants of *Pdgfa*, *Pdgfc*, and *Pdgfr*α shows that PDGF-A_{long} plays a role in intestinal organogenesis and possibly also in other developmental processes. However, this function is partly redundant with those of PDGF-A_{short} and PDGF-C.

MATERIALS AND METHODS

Generation of *Pdgfa* exon 6-deficient mice ($Pdgfa^{\Delta ex6/\Delta ex6}$). Mouse genomic *Pdgfa* clones were previously isolated from a 129Sv library (32). A HindIII-HindIII fragment containing exon 6 was subcloned into the p-Alter plasmid. The 5′ splice site of exon 6 was replaced with an EcoRI site by site-specific mutagenesis (Altered Sites II *in vitro* mutagenesis system Q6210; Promega Inc.). Mutated sequences were confirmed by sequencing. A 2.0-kb *loxP*-flanked PGK-neo selection marker (ploxPneo-1, a gift from Janet Rossant, Hospital for Sick Children Research Institute, Toronto, Canada) was blunt-end cloned into a PstI site of intron 5. Finally, a BamHI-HindIII fragment of intron 5 was added to the 5′ end of the construct, resulting in a total of 7.5 kb of sequence homology to the *Pdgfa* gene. The final $Pdgfa^{\Delta ex6}$ construct was electroporated into R1 (129Sv) embryonic stem (ES) cells (http://www.mshri.on.ca/nagy/r1.htm). Correct targeting of the *Pdgfa* allele was confirmed in ~10% of the ES cell clones by Southern blot analysis. Standard methods were used for microinjection of $Pdgfa^{\Delta ex6/+}$ ES cells into C57BL6 blastocysts and further generation of gene-targeted mice. Mice were used either on a mixed genetic background (129Sv × C57BL6) or on a background enriched for C57BL6/J DNA. Mice were bred and handled in accordance with Swedish animal welfare legislation, and all experiments were approved by the committees for animal ethics in Göteborg and Stockholm North.

Genotyping. The $Pdgfa^{\Delta ex6}$ allele was initially identified by Southern blotting in ES cells and founder mice. Genomic DNA was digested by EcoRI and subjected to standard Southern blot techniques. Hybridization with a ^{32}P-labeled 900-bp HindIII-BamHI fragment resulted in the expected bands of 18.5 kb (wild type) and 10.8 kb (mutant). A routine PCR genotyping protocol was subsequently developed. Wild-type (185-bp) and mutant (147-bp) bands were identified using 5′ AACAACATTCAG GCAGCCC and 5′ TTACCTGATTCCCTACGCC primers. $Pdgfr\alpha^{GFP/+}$ mice were genotyped by analysis of tissue fluorescence under a UV lamp with confirmation by PCR, as described previously (33). The *Pdgfa*-null allele ($Pdgfa^{-}$) was identified by PCR, as described previously (34). For *Pdgfc*, wild-type (185-bp) and null (389-bp) alleles were identified using 5′ AGCTGACATTTGATGAGAGAT, 5′ AGTAGGTGAAATAAGAGGT GAACA, 5′ CTCATGTTCTCGTGACTCTGA, and 5′ TAGCTAGTCGA TACCGTCGA primers.

RNA preparation. Freshly dissected tissues from wild-type and $Pdgfa^{\Delta ex6/\Delta ex6}$ mice were put in RNAlater (Ambion) and stored at −70°C before RNA preparation. Total RNA was extracted using the RNeasy Mini kit (Qiagen). RNA quality and concentration were analyzed in a 2100 Bioanalyzer instrument (Agilent Technologies, Santa Clara, CA).

Northern blot analysis. Total RNA from postnatal day 1 (P1) whole-mouse tissue was prepared and poly $(A)^+$ purified (RNeasy Midi and Oligotex mRNA kits; Qiagen Inc.), followed by blotting (Northern Max kit; Ambion Inc.). Full-length *Pdgfa* and *Pdgfc* cDNAs were used as probes. The strength of individual *Pdgfa* and *Pdgfc* bands in $Pdgfa^{\Delta ex6/\Delta ex6}$ and $Pdgfa^{-/-}$ lanes was normalized against *beta-actin* and *Gapdh* signals and compared to the wild-type expression levels using NIH Image 1.62 software.

Q-PCR. The RNA preparation was treated with DNase I, followed by reverse transcription (RT) with the SuperScript III first-strand synthesis System for RT-PCR (Invitrogen), using a combination of oligo(dT) primers and random primers. An extra reaction was run without the enzyme as a negative control. We used the following TaqMan gene expression assays from Applied Biosystems (Foster City, CA); *mPdgfa* exon 2-3 (Mm00435540_m1), *mPdgfa* exon 5-6 (Mm01201046_g1), and *mPdgfa* exon 5-7 (Mm01205760_m1). Mouse *Gapdh* (Mm99999915_g1) was used as an endogenous control, and all samples were used in triplicate in the PCR. Quantitative real-time PCR (Q-PCR) was performed according to protocols provided by Applied Biosystems, and the comparative threshold cycle (C_t) method ($\Delta\Delta C_t$ quantitation) was used to calculate the fold change between samples.

RT-PCR. Total RNA from different organs in P1.5 wild-type mice was used as the template for reverse transcription with an oligo(dT) primer and Superscript II reverse transcriptase (Life Technologies, Inc.). PCR was performed using a forward primer corresponding to *Pdgfa* exon 5 (5′ GCAAGACCAGGACGGTCATTTAC) and a reverse primer corresponding to exon 7 (5′ TGTTCAGGAATGTCACACGCC). The presence of

exon 6 resulted in a 434-bp band ($Pdgfa_{long}$), and the absence of exon 6 resulted in a 365-bp band ($Pdgfa_{short}$).

Histological techniques. Mice were anesthetized and perfused through the heart with Hanks' balanced salt solution (HBSS), followed by 4% buffered paraformaldehyde. For analysis of the intestine, care was taken to also wash out the intestinal lumen content with fixative. Dissected tissues were postfixed overnight at +4°C. For paraffin sectioning, tissues were first dehydrated in a series of ethanol according to standard methods. Five- to 7-μm sections were stained with Mayer's hematoxylin and eosin, and pictures were taken in a Nikon Eclipse E800 microscope. For cryosectioning, tissues were soaked in 30% sucrose and embedded in Tissue-Tek O.C.T. Compound (Sakura). Frozen sections were stained with 5 μg/ml FM4-64FX membrane dye (Invitrogen), and pictures were taken in a Zeiss LSM700 confocal microscope.

Quantification of lung alveolar density. Thirteen $Pdgfa^{\Delta ex6/-}$; $Pdgfr\alpha^{GFP/+}$ and 12 $Pdgfa^{+/-}$; $Pdgfr\alpha^{GFP/+}$ littermate controls from time points between P4 and P390 were divided into four different groups (P4 to P30, P60 to P90, P100 to P215, and P240 to P390). Lungs were fixed as described above and embedded in paraffin, sectioned, and counterstained with hematoxylin and eosin. Bright-field images from three different areas of each lung were taken at ×20 magnification. For each lung, the area with the sparsest alveolar network was chosen for quantification. The number of open areas and their perimeters were determined using NIS-Elements BR2.3. Statistics were calculated with an unpaired Student's *t* test.

Quantification of *PDGFR*α-positive cells in the spinal cord. Embryonic day 15.5 (E15.5) embryos with the following genotypes were fixed and embedded in OCT, as described above: $Pdgfa^{-/-}$; $Pdgfr\alpha^{GFP/+}$, $Pdgfa^{+/-}$; $Pdgfr\alpha^{GFP/+}$, $Pdgfa^{+/+}$; $Pdgfr\alpha^{GFP/+}$, and $Pdgfa^{\Delta ex6/\Delta ex6}$; $Pdgfr\alpha^{GFP/+}$. A series of 15 to 20 consecutive horizontal sections (containing cross sections of the spinal cord) were collected from each embryo and viewed in the confocal microscope. To ensure that the same level of the spinal cord was analyzed in the different mutants, the series of sections started with the most anterior section in which the heart appeared, and consecutive sections were taken in an anterior-posterior orientation. The green fluorescent protein (GFP)-positive cells in the spinal cords were counted, and the spinal cord areas were measured for each section in Volocity 5 (Improvision). A mean value for all sections in each embryo was calculated and expressed as GFP^+ cells per area. Statistics were calculated using Student's *t* test.

Analysis of albuminuria. Spontaneously voided spot urine was collected and analyzed for albuminuria by loading 1-μl samples on individual lanes of a 4 to 12% Tris gel. Bovine serum albumin (BSA) standards were loaded at 0.5, 1, and 5 μg/μl. The Thermo Scientific PageRuler prestained protein ladder was loaded as a size marker. Gels were stained using Coomassie blue.

RESULTS

Abundances of $Pdgfa_{long}$ and $Pdgfa_{short}$ transcripts in different mouse tissues. Alternative splicing of the *Pdgfa* transcript gives rise to either a short, freely diffusible protein (PDGF-A_{short}), or a long, ECM-associated protein (PDGF-A_{long}). We examined the relative expression levels of the two different transcripts in lung, liver, kidney, intestine, brain, heart, and skin in P4 wild-type mice, i.e., in organs where expression and/or function of PDGF-A has been demonstrated (8). To be able to compare the relative expression levels of the $Pdgfa_{long}$ and $Pdgfa_{short}$ transcripts in different tissues, we performed RT-PCR with primers spanning between exon 5 and exon 7, generating different-size products corresponding to $Pdgfa_{long}$ and $Pdgfa_{short}$ competitively in the same PCR (Fig. 1A). This analysis showed that $Pdgfa_{short}$ is the predominant *Pdgfa* transcript in most tissues, a finding consistent with previous data on human *PDGFA* clone abundance in cDNA libraries (18). The largest relative amount of $Pdgfa_{long}$ was observed in the intestine, where it represents approximately half of the total *Pdgfa* mRNA (Fig. 1A).

The expression levels of *Pdgfa* mRNA in different organs were also assessed by Q-PCR using TaqMan assays. Three TaqMan assays detecting different exon boundaries were applied; exon 2-3 and exon 5-7 assays, which detect all *Pdgfa* transcripts (total *Pdgfa*), and an exon 5-6 assay, which detects only $Pdgfa_{long}$. Since the efficiencies of different TaqMan assays vary, we normalized the data against the intestinal levels of *Pdgfa* mRNA. Since approximately half of the intestinal *Pdgfa* mRNA is $Pdgfa_{long}$ and half $Pdgfa_{short}$ (Fig. 1A), we set intestinal levels of total *Pdgfa* arbitrarily to 1 and levels of $Pdgfa_{long}$ to 0.5 (Fig. 1B). This allowed an approximate comparison of $Pdgfa_{long}$ with total *Pdgfa* mRNA levels across organs and revealed that the highest level of total *Pdgfa* mRNA occurs in the lung, followed by kidney, skin, intestine, brain, heart, and liver (Fig. 1B). The highest level of $Pdgfa_{long}$ was also observed in the lung, followed by intestine, kidney, skin, liver, and heart. $Pdgfa_{long}$ was undetectable in the brain.

In summary, mRNA analysis by competitive and quantitative PCR showed that most of the *Pdgfa* mRNA produced in the mouse is $Pdgfa_{short}$ and that both relative and absolute levels of $Pdgfa_{long}$ vary in a tissue-specific manner. Currently, no methods exist that allow specific identification of the individual PDGF-A protein isoforms in whole tissues.

***Pdgfa*$^{\Delta ex6/\Delta ex6}$ mice are viable and fertile.** As demonstrated above, $Pdgfa_{long}$ mRNA is detectably expressed in most but not all organs. To find out if $Pdgfa_{long}$ is required for any specific developmental process(es), we generated mice in which splicing into exon 6 was disrupted. The splice acceptor site in exon 6 and the adjoining 5′ polypyrimidine tract were deleted by site-directed mutagenesis of a gene-targeting construct (Fig. 1C and D), and the mutation was subsequently introduced by homologous recombination into mouse ES cells. Heterozygous *Pdgfa* exon 6-deficient mice ($Pdgfa^{\Delta ex6/+}$) were derived and bred to homozygosity ($Pdgfa^{\Delta ex6/\Delta ex6}$) (Fig. 1E and F). In contrast to total *Pdgfa*-null ($Pdgfa^{-/-}$) mice, which invariably die between midgestation and early postnatal age (32), $Pdgfa^{\Delta ex6/\Delta ex6}$ mice were born in Mendelian frequencies, survived into adulthood, and were fertile and overall healthy.

We failed to detect any residual splicing into exon 6 in $Pdgfa^{\Delta ex6/\Delta ex6}$ mice by Q-PCR (Fig. 1G) and RT-PCR (Fig. 1H) analyses of different tissues. We therefore conclude that only the PDGF-A_{short} mRNA is generated in $Pdgfa^{\Delta ex6/\Delta ex6}$ mice. PDGF-A and PDGF-C are partially redundant ligands for PDGFRα. To test if the mutagenesis of *Pdgfa* resulted in changes in the levels of *Pdgfc* mRNA through putative common feedback regulatory mechanisms, we analyzed *Pdgfc* expression by Northern blotting of mRNA prepared from whole $Pdgfa^{-/-}$ and $Pdgfa^{\Delta ex6/\Delta ex6}$ P1 pups (Fig. 2A) and by Q-PCR on individual organs (brain, lung, heart, kidney, liver, intestine, and skin) at P10 and P30 (data not shown). Neither of these methods demonstrated any significant change in the levels of *Pdgfc* mRNA in $Pdgfa^{\Delta ex6/\Delta ex6}$ mutants, and Northern blot analysis also failed to reveal any upregulation of *Pdgfc* mRNA in $Pdgfa^{-/-}$ mice (Fig. 2A).

Analysis of potential hypomorphic properties of the *Pdgfa*$^{\Delta ex6}$ allele. Targeted mutagenesis of endogenous genes sometimes results in unintended reduction of their transcription efficiency because unknown transcription-regulatory domains are deleted, resulting in hypomorphic alleles (35, 36). Hypomorphism may also result from transcriptional interference with the

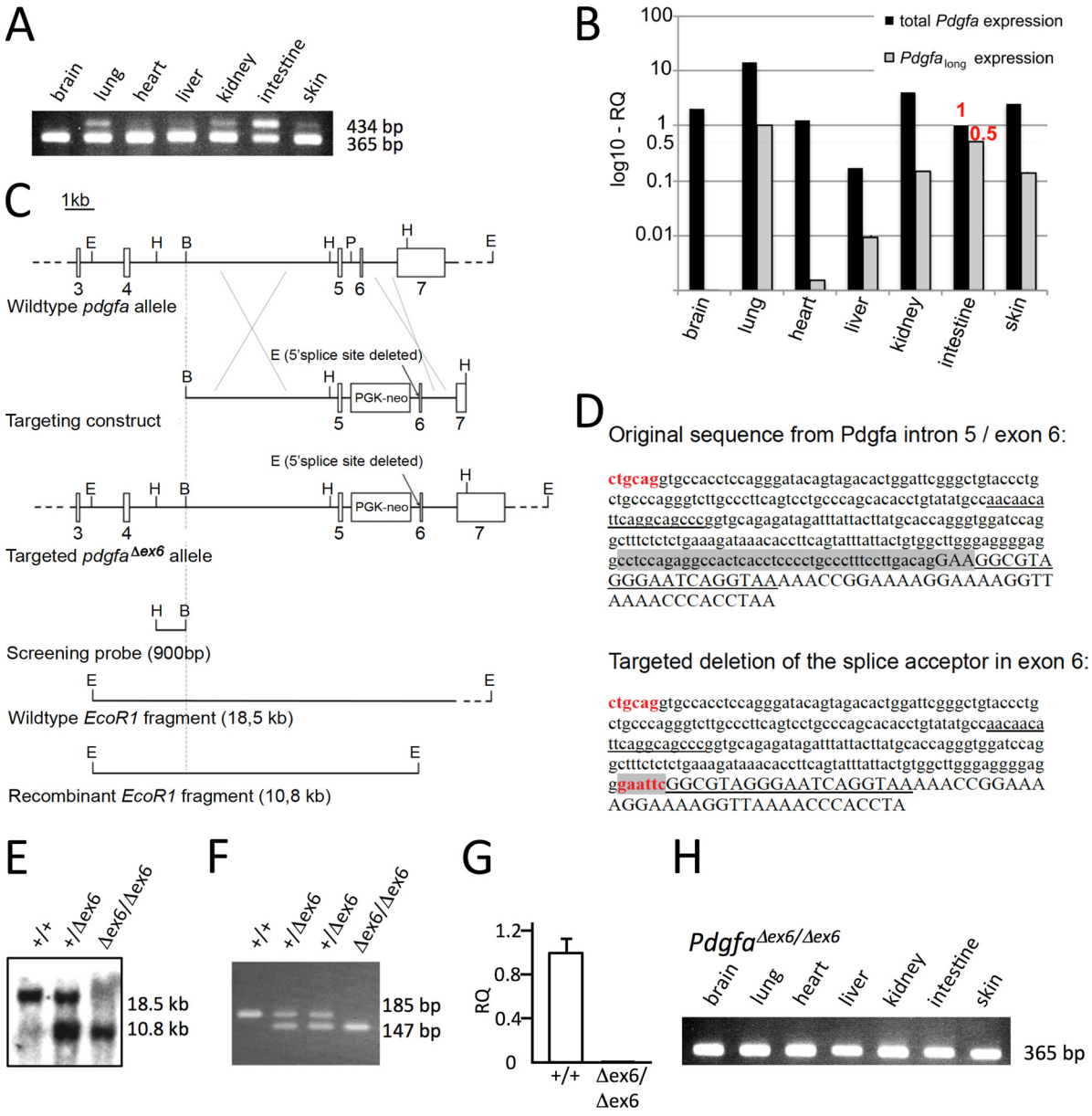

FIG 1 Expression of *Pdgfa* in wild-type tissues and generation of mice lacking the PDGF-A retention motif. (A) RT-PCR on tissues from P1 wild-type C57BL/6 mice using primers in exon 5 and exon 7. Amplification from $Pdgfa_{long}$ resulted in a 434-bp fragment and amplification from $Pdgfa_{short}$ in a 365-bp fragment. The highest relative levels of $Pdgfa_{long}$ were found in the intestine, where it made up 50% of the total *Pdgfa* levels. The image shown is representative of analyses done on 3 mice. (B) Q-PCR on RNA from different tissues from a P4 wild-type C57BL/6 mouse. Total expression of *Pdgfa* mRNA was quantified with primers in exon 2 and exon 3. The long *Pdgfa* transcript was quantified using primers in exon 5 and exon 6. The red numbers indicate the relative levels to which other values were normalized according to the RT-PCR levels in the intestine, where $Pdgfa_{long}$ made up 50% of the total *Pdgfa*, as shown in panel A. The *y* axis shows $\log_{10}$ relative quantitation (RQ). The values are the means of three technical repeats representing independent rounds of mRNA preparation and cDNA synthesis. (C) Outline of the $Pdgfa^{\Delta ex6}$ targeting strategy. Exon numbers are indicated. Letters refer to restriction sites: E, EcoRI; H, HindIII; B, BamHI; P, PstI. (D) (Top) Sequence of the mouse *Pdgfa* intron 5-exon 6 boundary. Uppercase letters indicate exons, and lowercase letters indicate introns. The PstI site where the neomycin gene was introduced is depicted in red letters. The exon 6 splice acceptor and the adjacent polypyrimidine tract are shaded. (Bottom) The exon 6 splice acceptor was deleted and an EcoRI recognition sequence was introduced for Southern blot analysis (shaded). The underlined sequences represent PCR primers for genotyping. (E) Southern blot genotyping with probe and restriction enzyme digestion shown in panel C. (F) PCR of wild-type (+/+), heterozygous (Δex6/+), and homozygous (Δex6/Δex6) *Pdgfa* exon 6-deficient mice. (G) Q-PCR on $Pdgfa^{\Delta ex6/\Delta ex6}$ and wild-type lung tissue at P30 ($n = 4$; C57BL6 background; statistics by *t* test) using primers in exon 5 and exon 6 showing that no splicing into exon 6 occurs in $Pdgfa^{\Delta ex6/\Delta ex6}$ mice. The error bar represents the standard deviation. (H) RT-PCR on tissues from P1 $Pdgfa^{\Delta ex6/\Delta ex6}$ mice on a mixed C57BL6/129sv background using primers in exon 5 and exon 7 revealed only the expected 365-bp band from $Pdgfa_{short}$. (H) Gel representative of analyses done on 3 mice.

antibiotic resistance selection gene if it remains in the recombinant allele. Since the latter is the case for $Pdgfa^{\Delta ex6}$ (Fig. 1C), we quantified the transcription efficiency of the $Pdgfa^{\Delta ex6}$ allele in comparison to the wild-type allele. Northern blot analysis of whole-animal RNA prepared from P1 pups did not reveal hypomorphic expression of *Pdgfa* mRNA from the $Pdgfa^{\Delta ex6}$ allele, but rather, generated overall levels of *Pdgfa* mRNA similar to or slightly increased in comparison with the wild-type allele

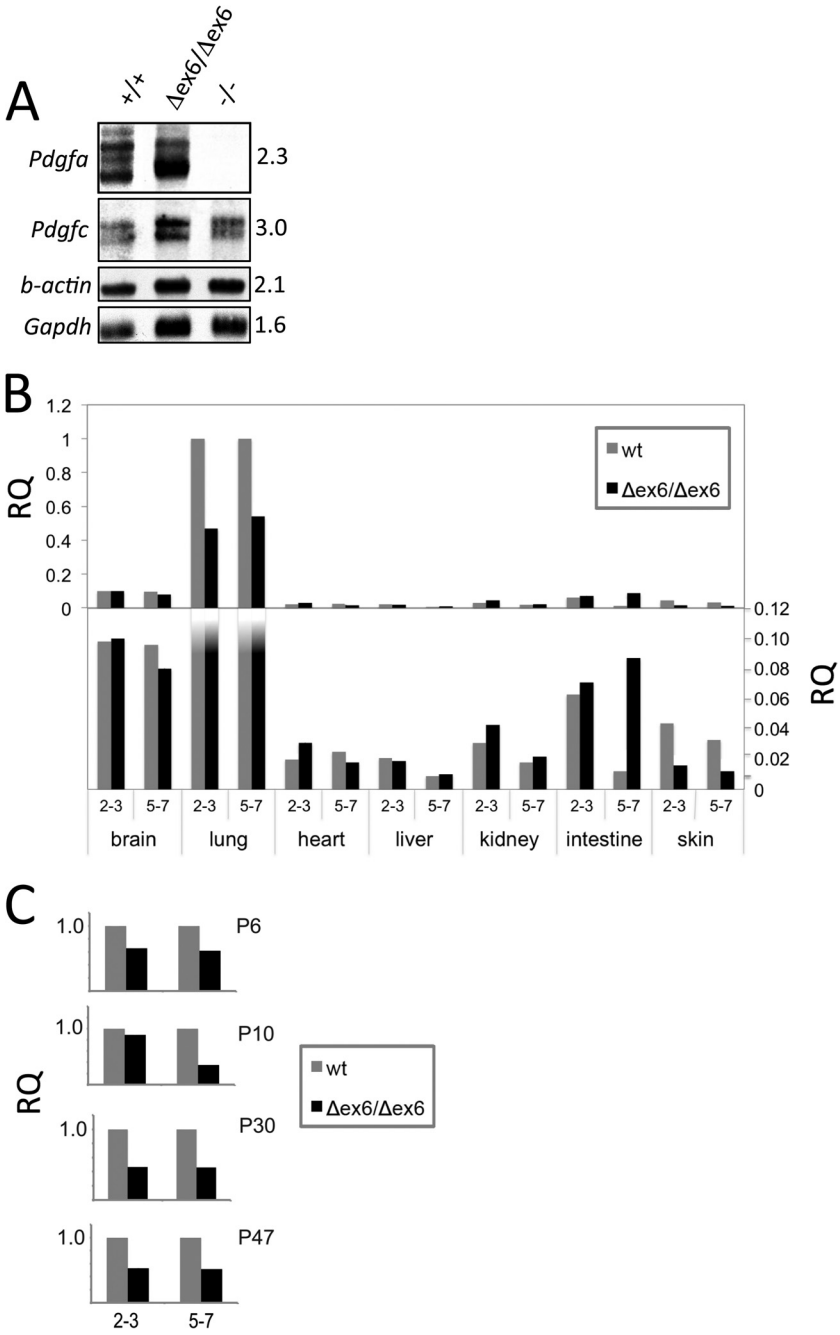

FIG 2 Analysis of *Pdgfa* mRNA levels. (A) Northern blot analysis of RNA prepared from whole newborn mice of the indicated *Pdgfa* genotypes. Hybridization probes are shown on the left and size (kb) on the right. Image analysis after normalization to β-*actin* and *Gapdh* mRNAs suggested comparable levels of *Pdgfa* and *Pdgfc* mRNAs in $Pdgfa^{\Delta ex6/\Delta ex6}$ pups. (B) Q-PCR on tissues from different organs at P47, using primers for exon 2 and exon 3 (2-3) and for exon 5 and exon 7 (5-7). In the upper graph, relative quantitation is shown on the *y* axis on the left. The lower graph shows the same data at a different scale, with relative quantification levels on the right. The transcription efficiency of *Pdgfa* in the lung showed a 50% reduction in $Pdgfa^{\Delta ex6/\Delta ex6}$ compared to wild-type mice. In the intestine, the opposite effect was indicated, the interpretation of which is discussed in Results in the text. (C) Q-PCR data from lung tissue at P6, P10, P30, and P47, using primer pairs for exon 2 and exon 3 (2-3) and for exon 5 and exon 7 (5-7). At all ages, transcript levels were reduced by about 50% in $Pdgfa^{\Delta ex6/\Delta ex6}$ mice. In panels B and C, the *y* axis shows quantitation relative to wild-type mice. For panels A to C, $n = 1$ for each genotype on a C57BL6 background, except panel A, which was done on a mixed C57BL6/129sv background. The values represent means of three technical replicates. wt, wild type.

(Fig. 2A). To obtain a more quantitative analysis of the *Pdgfa* mRNA levels in different organs, we performed Q-PCR analysis on a panel of tissues from $Pdgfa^{\Delta ex6/\Delta ex6}$ and wild-type P47 littermates using TaqMan analyses across *Pdgfa* exons 2-3 and 5-7, respectively (the latter analysis spanned the mutated area) (Fig. 2B). The results of these analyses indicated similar *Pdgfa* mRNA levels between $Pdgfa^{\Delta ex6/\Delta ex6}$ and wild-type mice in most organs, but we noticed an approximately 50% reduction of *Pdgfa* mRNA levels in lung and skin from $Pdgfa^{\Delta ex6/\Delta ex6}$ mice (Fig. 2B). Slightly variable, but overall similar, results were obtained with

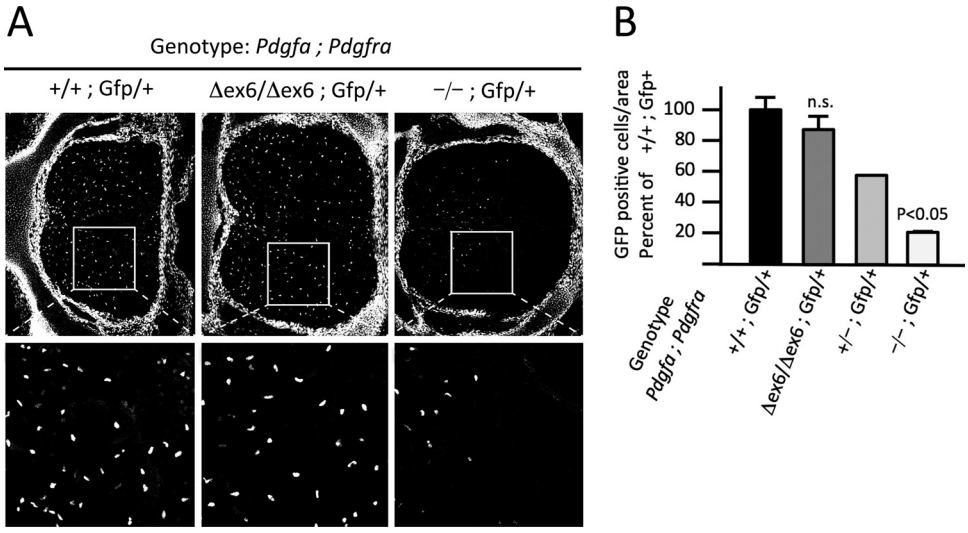

FIG 3 PDGFRα-positive cells in the embryonic spinal cord. (A) Spinal cords from E15.5 embryos of the indicated genotypes in a C57BL6 background analyzed for *Pdgfr*α-GFP expression. The images in the bottom row are enlargements of the boxed areas in the images above. (B) Quantification of GFP-positive cells per area in the spinal cords of $Pdgfa^{+/+}$; $Pdgfr\alpha^{GFP/+}$ ($n = 5$), $Pdgfa^{\Delta ex6/\Delta ex6}$; $Pdgfr\alpha^{GFP/+}$ ($n = 4$), $Pdgfa^{+/-}$; $Pdgfr\alpha^{GFP/+}$ ($n = 1$), and $Pdgfa^{-/-}$; $Pdgfr\alpha^{GFP/+}$ mice ($n = 2$). A minimum of 15 sections were analyzed for each mouse. Heterozygous and homozygous *Pdgfa* knockout mice showed reduced densities of GFP-positive cells. There was no significant difference between wild-type mice and $Pdgfa^{\Delta ex6/\Delta ex6}$; $Pdgfr\alpha^{GFP/+}$ mice. Statistics by Student's *t* test. The error bars represent standard deviations. n.s., not significant.

lung tissue from individuals at P6, P10, P30, and P47 (Fig. 2C). Treated as a group, the *Pdgfa* mRNA reduction in the lung was statistically significant in the $Pdgfa^{\Delta ex6/\Delta ex6}$ mice using the exon 5-7 analysis ($P < 0.005$); however, the exon 2-3 analyses did not reach significance at a *P* value of <0.05. Taken together, our results indicate that the $Pdgfa^{\Delta ex6}$ allele might be hypomorphic with regard to mRNA expression in the lung and skin, resulting in approximately 50% reduction of *Pdgfa* mRNA levels compared to the wild type. It is presently unclear if this reduction is the result of reduced transcription, decreased RNA stability, or both. Significantly reduced expression of the $Pdgfa^{\Delta ex6}$ allele was not observed in other tissues tested, including brain and intestine, two organs where the physiological role of *Pdgfa* has been analyzed previously (37, 38). In the intestine, the $Pdgfa^{\Delta ex6}$ allele showed a conspicuous increase in the exon 5-7 but not the exon 2-3 PCR product. This result may reflect the intestine's uniquely high relative levels of $Pdgfa_{long}$. In the absence of exon 6, the levels of $Pdgfa_{short}$ would be expected to double. The $Pdgfa_{short}$ product likely amplifies more efficiently than the $Pdgfa_{long}$ product in the 5-7 reaction because it is 69 bp shorter. Therefore, the observed increased level of the 5-7 product in the intestine might be expected, whereas no difference would be expected in the 2-3 reaction, as was also observed (Fig. 2B). In conclusion, the Q-PCR data suggest the possible occurrence of an organ-specific hypomorphism of the $Pdgfa^{\Delta ex6}$ allele, leading to approximately 50% reduction of *Pdgfa* mRNA levels in lung and skin, whereas *Pdgfa* mRNA levels appear unchanged in other tissues analyzed.

Changes in mRNA levels do not necessarily produce parallel changes in protein levels, and moreover, changes in protein levels do not necessarily cause phenotypic alterations. In the case of PDGF-A, previous studies have demonstrated that PDGFRα-positive cells in the spinal cord represent oligodendrocyte progenitors (OP), which depend on PDGF-A for their proliferation and spread (37, 39). Moreover, it has been shown that the density of PDGFRα-positive OP in the spinal cord at E15 is directly proportional to the levels of *Pdgfa* mRNA at this location and that $Pdgfa^{+/-}$ mice (with half of the wild-type *Pdgfa* gene dose) display approximately half the density of PDGFRα-positive OP in the spinal cord in comparison with wild-type ($Pdgfa^{+/+}$) littermates (39, 40). Since CNS tissues express only the short *Pdgfa* mRNA isoform (Fig. 1A and B), the density of PDGFRα-positive OP in the E15 spinal cord should reflect the functional status of the *Pdgfa* gene in the $Pdgfa^{\Delta ex6/\Delta ex6}$ mice in this tissue. We therefore analyzed the abundance of PDGFRα-positive OP in E15.5 spinal cords from mice with different genotypes (Fig. 3). $Pdgfa^{\Delta ex6}$ mice were crossed with a $Pdgfr\alpha^{GFP}$ knock-in mouse (33) in order to facilitate identification of PDGFRα-positive cells by nuclear localization of GFP (33). The $Pdgfr\alpha^{GFP}$ allele is also a *Pdgfr*α-null allele and was therefore analyzed in heterozygotes ($Pdgfr\alpha^{GFP/+}$). We confirmed previously published results (37, 39) by first showing a gradual decrease in PDGFRα-positive cells in the E15.5 spinal cord of $Pdgfa^{+/-}$; $Pdgfr\alpha^{GFP/+}$ and $Pdgfa^{-/-}$; $Pdgfr\alpha^{GFP/+}$ mice compared to control ($Pdgfa^{+/+}$; $Pdgfr\alpha^{GFP/+}$) mice; the density of PDGFRα-positive cells was reduced by 40% in $Pdgfa^{+/-}$; $Pdgfr\alpha^{GFP/+}$ mice and by 77% in $Pdgfa^{-/-}$; $Pdgfr\alpha^{GFP/+}$ mice (Fig. 3A and B). However, there was no significant difference in the densities of PDGFRα-positive cells in the spinal cords of $Pdgfa^{\Delta ex6/\Delta ex6}$; $Pdgfr\alpha^{GFP/+}$ and $Pdgfa^{+/+}$; $Pdgfr\alpha^{GFP/+}$ embryos (Fig. 3A and B). These results provide biological evidence suggesting that the $Pdgfa^{\Delta ex6}$ allele is not functionally hypomorphic at a general level or specifically in the spinal cord.

Progressive loss of lung alveoli in $Pdgfa^{\Delta ex6}$ mutants. The lung is an organ strongly affected by the complete loss of PDGF-A (32, 34, 41). Since the highest levels of the $Pdgfa_{long}$ transcripts were observed in the lung (Fig. 2B), we asked if $Pdgfa^{\Delta ex6}$ mutants displayed any specific lung phenotype. We hypothesized that the $PDGFA_{long}$ protein might be required to be in close proximity to the PDGF-A-producing epithelial cells, where it should be prevented from diffusing away by interacting with HSPGs.

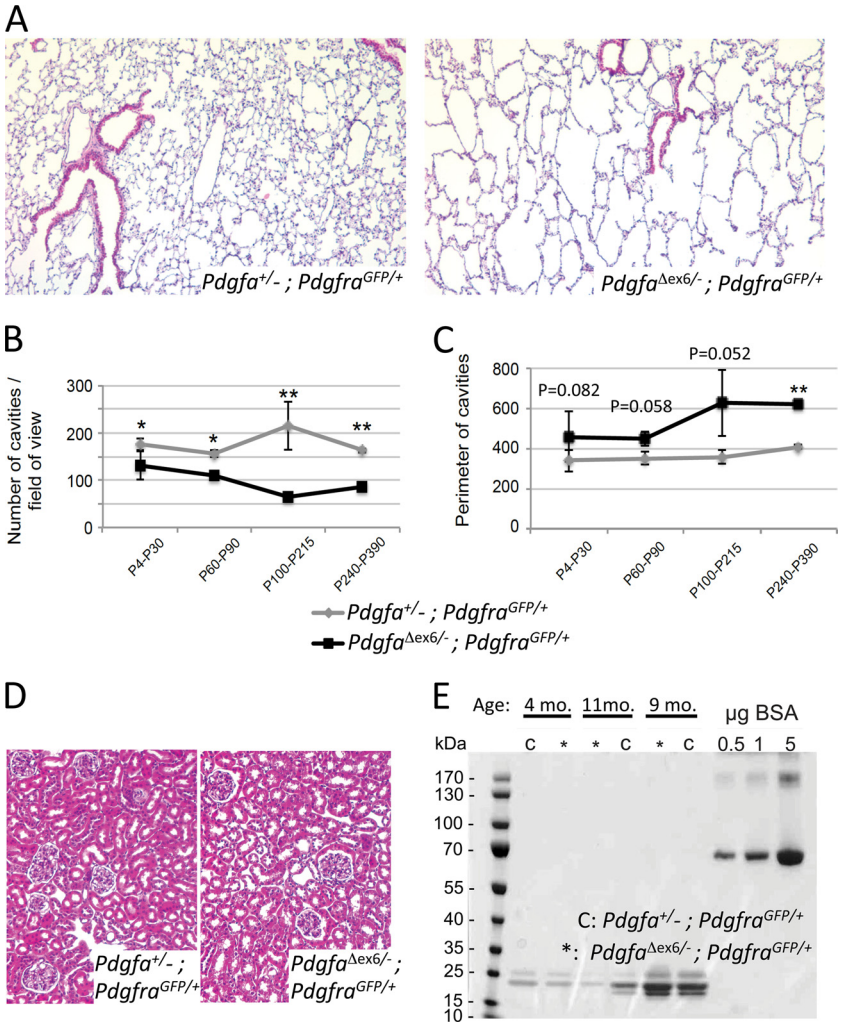

FIG 4 Phenotypic analysis of lung and kidney in *Pdgfa*$^{\Delta ex6/-}$; *Pdgfr*α$^{GFP/+}$ mice. (A) Mayers hematoxylin and eosin staining of lung tissue from P215 mice with the indicated genotypes in a C57BL6 background. (B) Quantification of the cavities in lungs from *Pdgfa*$^{\Delta ex6/-}$; *Pdgfr*α$^{GFP/+}$ and *Pdgfa*$^{+/-}$; *Pdgfr*α$^{GFP/+}$ mice of different ages. (C) Comparison of perimeters in cavities of lungs from *Pdgfa*$^{\Delta ex6/-}$; *Pdgfr*α$^{GFP/+}$ and *Pdgfa*$^{+/-}$; *Pdgfr*α$^{GFP/+}$ mice at different ages. For panels B and C, the same mice were analyzed, with each age group consisting of 3 littermate-matched pairs in a C57BL6 background. The error bars indicate standard deviations. *, $P < 0.05$; **, $P < 0.01$. (D) Mayers hematoxylin and eosin staining of kidneys from *Pdgfa*$^{\Delta ex6/-}$; *Pdgfr*α$^{GFP/+}$ and *Pdgfa*$^{+/-}$; *Pdgfr*α$^{GFP/+}$ mice at P215 ($n = 1$ per genotype). (E) Coomassie blue-stained gel run with spot urine samples from *Pdgfa*$^{\Delta ex6/-}$; *Pdgfr*α$^{GFP/+}$ mice (*) and *Pdgfa*$^{+/-}$; *Pdgfr*α$^{GFP/+}$ controls (c) at 4, 9, and 11 months of age ($n = 1$ per age and genotype). No proteins the size of albumin (compared to a BSA standard) or larger were found, irrespective of genotype. The observed variation in the abundances of low-molecular-mass proteins is expected in spot urine samples and is caused by variable urine concentrations.

However, we were not able to detect any lung abnormalities in *Pdgfa*$^{\Delta ex6/\Delta ex6}$ mice, even when combined with a heterozygous state for a *Pdgfr*α-null allele (*Pdgfa*$^{\Delta ex6/\Delta ex6}$; *Pdgfr*α$^{GFP/+}$) (data not shown). A further challenge was encountered in replacing one of the *Pdgfa*$^{\Delta ex6}$ alleles with a *Pdgfa*-null allele (*Pdgfa*$^{\Delta ex6/-}$; *Pdgfr*α$^{GFP/+}$). These mice were born at a Mendelian distribution and appeared healthy. In comparison with *Pdgfa*$^{+/-}$; *Pdgfr*α$^{GFP/+}$ mice, which were used as controls, the *Pdgfa*$^{\Delta ex6/-}$; *Pdgfr*α$^{GFP/+}$ mice displayed an abnormal lung morphology that consisted of dilated distal airways and reduced numbers of alveoli (Fig. 4A). This abnormality was apparent at all ages analyzed (P4 onward), but the phenotype progressed with age and developed into a lung emphysema-like histopathology at 3 months of age (Fig. 4A to C). These abnormalities were unevenly distributed in the lungs, and in order to facilitate quantitative analysis and compensate for possible differences in lung inflation during fixation, we consistently compared the most inflated lung regions. Quantification of the epithelium-enclosed cavities and their perimeters revealed a significant change in both parameters (Fig. 4B and C). In parallel, we identified a similar lung phenotype in *Pdgfa*$^{\Delta ex6/-}$; *Pdgfr*α$^{+/+}$ mice (data not shown), suggesting that the concentration of PDGF-A is critical for the development and maintenance of a normal lung alveolar structure in mice, whereas the concentration of PDGFRα is less important.

In contrast to the full *Pdgfa* knockouts (34), no reduction was observed in the mRNA levels for elastin in *Pdgfa*$^{\Delta ex6/-}$; *Pdgfr*α$^{GFP/+}$ lungs, as measured by TaqMan Q-PCR (data not shown). In addition, we did not observe any developmental abnormalities in other organs known to be abnormal in the complete absence of PDGF-A or PDGFRα, i.e., the gastrointestinal

tract or the skeleton (data not shown). For example, kidney histology was normal in *Pdgfa*$^{\Delta ex6/-}$; *Pdgfrα*$^{GFP/+}$ mice, including well-formed glomeruli, tubuli, and renal mesenchyme (Fig. 4D). Renal function appeared normal, since proteinuria—the leakage into urine of plasma proteins the size of albumin or greater—was not detected (Fig. 4E). Lung elastin production, intestinal villus formation, rib anatomy, and kidney mesenchyme development have all been shown to be abnormal in full *Pdgfa* and/or *Pdgfrα* knockout mutants (32, 38, 42, 43). The lack of any discernible effects of PDGF-A$_{long}$ deficiency on these processes may indicate that PDGF-A$_{long}$ is of specific importance during lung alveogenesis. An alternative explanation for the relatively high sensitivity of the lung to the loss of PDGF-A$_{long}$ in comparison with the kidney and intestine may be that the *Pdgfa*$^{\Delta ex6}$ allele is hypomorphic in the lung but not in the kidney and intestine (Fig. 2B). At present, it is difficult to distinguish between these possibilities.

Analysis of compound mutants suggests overlapping roles for PDGF-A and PDGF-C in the development of the vertebral column and the intestine. PDGF-A and PDGF-C have partly overlapping expression patterns and functions in mammalian development (8, 44), and they both bind to and activate PDGFRα. Double knockout of the *Pdgfa* and *Pdgfc* genes causes embryonic death with a phenotype similar to that of the full *Pdgfrα* knockout and significantly more severe than any of the single *Pdgfa* or *Pdgfc* knockout phenotypes (42). To reveal if PDGF-A$_{long}$ has any specific function that overlaps with that of PDGF-C, we generated *Pdgfa*$^{\Delta ex6/\Delta ex6}$; *Pdgfc*$^{-/-}$ double mutants. On a mixed 129sv/C57BL6 genetic background, double-mutant mice were born at Mendelian frequency but were 25% smaller than all of the control littermates on average (wild type, 93.4% [$n = 8$]; *Pdgfa*$^{\Delta ex6/\Delta ex6}$, 95.5% [$n = 14$]; *Pdgfa*$^{\Delta ex6/\Delta ex6}$; weights were normalized to the heaviest individual of the same sex in the same litter [100%] *Pdgfc*$^{+/-}$, 88.4% [$n = 20$]; *Pdgfa*$^{\Delta ex6/\Delta ex6}$; *Pdgfc*$^{-/-}$, 72.3% [$n = 11$]). On this background, all adult *Pdgfa*$^{\Delta ex6/\Delta ex6}$; *Pdgfc*$^{-/-}$ mice ($n = 11$) displayed spina bifida, which was macroscopically visible upon dissection. A proportion (3/11) of the *Pdgfa*$^{\Delta ex6/\Delta ex6}$; *Pdgfc*$^{-/-}$ mice developed severe kyphosis of the thoracic spine (Fig. 5A, D, and E) and partial paralysis of the hind legs. Others had milder spina bifida (spina bifida occulta) without external signs and first visible during dissection. This heterogeneity prompted us to generate *Pdgfa*$^{\Delta ex6/\Delta ex6}$; *Pdgfc*$^{-/-}$ mice in a pure C57BL/6 background (>10-generation backcross). In this genetic background also, the penetrance of spina bifida was 100%, but heterogeneity was observed, with the most severe case (1/5) presenting as an ulcerating stripe along the spine in newborns. Other cases displayed a milder but still externally visible spina bifida (2/5) or spina bifida occulta visible only during dissection (2/5). Spina bifida occulta was also observed in newborn *Pdgfc*$^{-/-}$ mice in a C57BL/6 background (data not shown), as well as in *Pdgfc*$^{-/-}$ adults in a mixed genetic background (Fig. 5C). We did not observe spina bifida of any degree in *Pdgfa*$^{\Delta ex6/\Delta ex6}$ mice (Fig. 5B). Interestingly, *Pdgfa*$^{+/-}$; *Pdgfc*$^{-/-}$ mutants displayed fully penetrant spina bifida in newborns that was more severe than in the other mutants analyzed (3/3 cases) (Fig. 5F). This suggests a strict dosage sensitivity of PDGF-A in the absence of PDGF-C for vertebral development. We did not assess the expression level of the *Pdgfa*$^{\Delta ex6}$ allele in the developing vertebral column. However, since the most penetrant severe spina bifida was observed in *Pdgfa*$^{+/-}$; *Pdgfc*$^{-/-}$ rather than in *Pdgfa*$^{\Delta ex6/\Delta ex6}$; *Pdgfc*$^{-/-}$ mice, the *Pdgfa*$^{\Delta ex6}$ allele is likely less hypomorphic in the developing vertebral column than in the lung, since *Pdgfa*$^{+/-}$; *Pdgfc*$^{-/-}$ mice would otherwise have been expected to be phenotypically similar to *Pdgfa*$^{\Delta ex6/\Delta ex6}$; *Pdgfc*$^{-/-}$ mice.

Further histological analyses of *Pdgfa*$^{\Delta ex6/\Delta ex6}$; *Pdgfc*$^{-/-}$ mice were performed with a focus on tissues known to require PDGF-A for their development. We did not detect any abnormalities in lung, CNS, skin, or testis (data not shown). Interestingly, however, the upper small intestine of *Pdgfa*$^{\Delta ex6/\Delta ex6}$; *Pdgfc*$^{-/-}$ mice postweaning displayed a phenotype that was highly similar to the one reported for *Pdgfa*$^{-/-}$ mice (38) (Fig. 5J and K). We performed this analysis in a mixed 129sv/C57BL6 genetic background to allow comparison with *Pdgfa*$^{-/-}$ mice, which are prenatal or perinatal lethal in a C57BL6-enriched background. Gastrointestinal villi were abnormally shaped and reduced in number (Fig. 5J and K), and a pronounced thinning of the submucosal mesenchyme was observed (Fig. 5L to N). The intestine has the highest relative expression of *Pdgfa*$_{long}$ (Fig. 1A) and did not display expression hypomorphism of the *Pdgfa*$^{\Delta ex6}$ allele (Fig. 2B), suggesting that the observed intestinal phenotype represents a specific role of PDGF-A$_{long}$ in this organ. Nevertheless, the fact that none of the *Pdgfa*$^{\Delta ex6/\Delta ex6}$ single mutants showed this phenotype indicates that PDGF-C has the ability to compensate for the loss of PDGF-A$_{long}$ in the intestines of *Pdgfa*$^{\Delta ex6/\Delta ex6}$ mice.

DISCUSSION

PDGF-A is widely expressed in epithelial, muscular, and nervous tissues during development and plays multiple roles in the development of a number of tissues and organs (reviewed in references 8 and 21). In the mouse, and probably in all mammals, PDGF-A plays a role in the formation of neural-crest-derived mesenchyme in the heart and head regions (43); in mesenchymal development in multiple epithelial organs, including lung (32, 34, 41), intestine (38), skin (45), testis (46), and kidney (42); and in the formation of oligodendrocytes (37) and retinal astrocytes (1).

The original cloning of *PDGF-A* from a human glioblastoma cDNA library demonstrated the existence of two alternatively spliced mRNA species, encoding PDGF-A proteins differing by the presence or absence of a C-terminal stretch of mostly basic amino acid residues (18). Subsequent analysis of the human *PDGF-A* gene structure revealed that the long PDGF-A isoform resulted from the alternative usage of a specific exon (exon 6) in the *PDGF-A* gene (17). An initial report suggested that splicing into exon 6 was tumor specific (24), but subsequent analysis demonstrated expression of *PDGF-A*$_{long}$ in both normal and neoplastic tissues (22). However, the relative abundances of *PDGF-A*$_{long}$ and *PDGF-A*$_{short}$ mRNA species vary between cell lines and tissues (47, 48), suggesting tissue-specific regulation of *PDGF-A* splicing.

This notion is supported by our present analysis of absolute and relative abundances of the different *Pdgfa* mRNA species in the developing mouse. Our analysis indicates the highest absolute abundance of *Pdgfa*$_{long}$ mRNA in the lung. This observation is consistent with the lung phenotype observed in *Pdgfa*$^{\Delta ex6/-}$; *Pdgfrα*$^{GFP/+}$ mutants, whereas other organs appeared normal in these mutants. The lack of detectable lung abnormalities in P*dgfa*$^{\Delta ex6/\Delta ex6}$ mutants may be explained by the high overall PDGF-A expression in this organ and, potentially, by compensation for loss of PDGF-A$_{long}$ by the high levels of PDGF-A$_{short}$ in the lung. This conclusion is supported by the fact that P*dgfa*$^{\Delta ex6/-}$ mutants demonstrated lung alveolar defects, since these mice not only lack PDGF-A$_{long}$ but also have reduced PDGF-A$_{short}$ levels. In

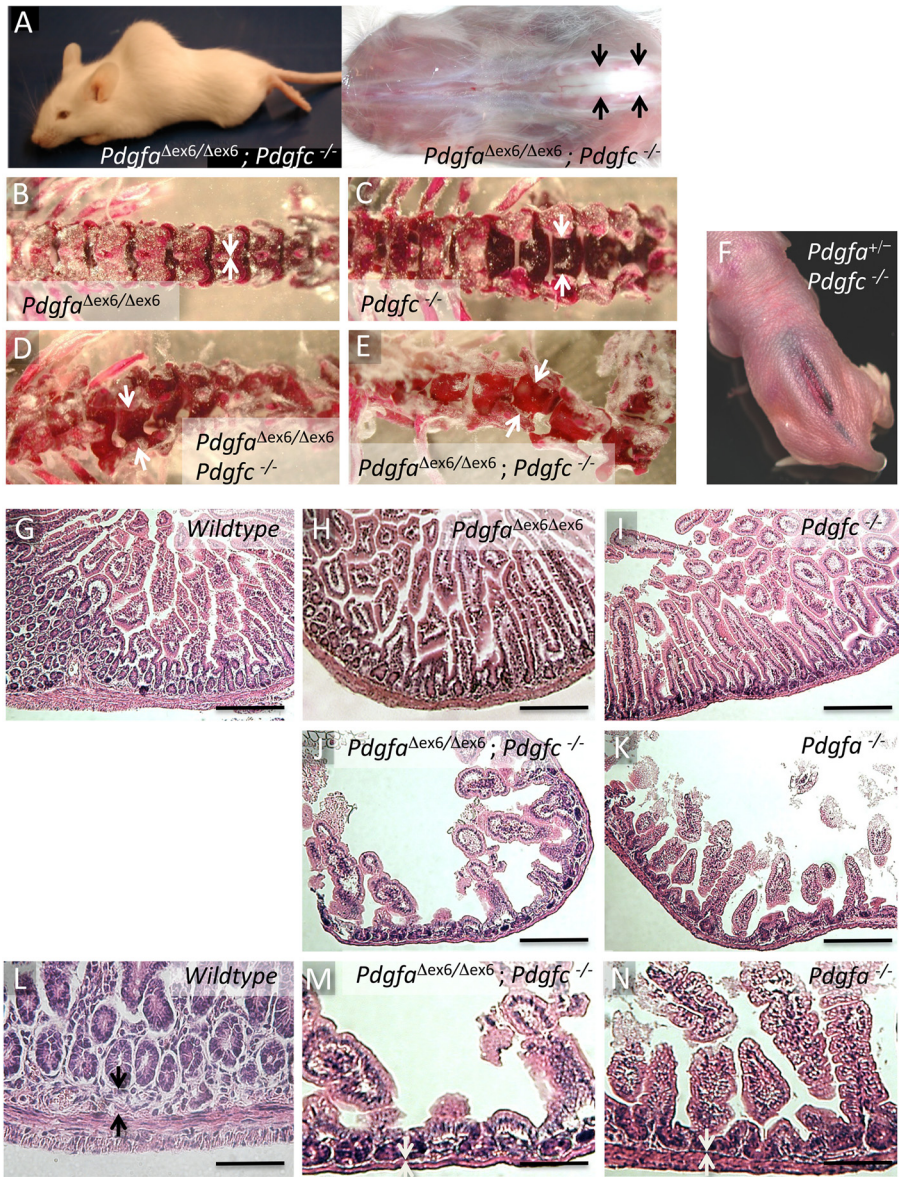

FIG 5 A compensatory role for PDGF-C in *Pdgfa*$^{\Delta ex6/\Delta ex6}$ mice. (A) Kyphosis in a *Pdgfa*$^{\Delta ex6/\Delta ex6}$; *Pdgfc*$^{-/-}$ mouse at P45 (left) and spina bifida revealed upon dissection (right). The arrows indicate white spinal cord tissue not fully enclosed by vertebrae in the lumbar region. (B to E) Skeletal preparations revealing intact vertebrae in *Pdgfa*$^{\Delta ex6/\Delta ex6}$ mice (B), mild spina bifida in *Pdgfc*$^{-/-}$ mice (C), and severe spina bifida in two *Pdgfa*$^{\Delta ex6/\Delta ex6}$; *Pdgfc*$^{-/-}$ mice (D and E). The arrows point to the midline of the dorsal vertebral arch. Note the missing dorsal arch of horseshoe-shaped affected vertebrae in panels C to E. Panels A to E are representative of analysis performed on a minimum of 8 mice per genotype from a mixed C57BL6/129sv background. (F) Ulceration over the dorsal back of a newborn *Pdgfa*$^{+/-}$; *Pdgfc*$^{-/-}$ mouse indicating severe spina bifida. The image is representative of 3 mice on a C57BL6 background. (G to N) Hematoxylin and eosin staining of the upper small intestine in early-postweaning mice (P17 to P19) with the indicated genotypes. Note the smaller number of villi in the upper small intestine in *Pdgfa*$^{\Delta ex6/\Delta ex6}$; *Pdgfc*$^{-/-}$ (J) and *Pdgfa*$^{-/-}$ (K) mice. *Pdgfa*$^{\Delta ex6/\Delta ex6}$ and *Pdgfc*$^{-/-}$ mice show normal intestinal morphology (H and I) comparable to that of the wild type (G). Higher-magnification views (L and M) show reduced thickness of the submucosal mesenchyme in *Pdgfa*$^{\Delta ex6/\Delta ex6}$; *Pdgfc*$^{-/-}$ (M) and *Pdgfa*$^{-/-}$ (N) mice compared to the wild type (L). Pairs of arrows (in panels L to N) show the thickness of the submucosal mesenchyme. The images in panels G to N are representative of analyses done on a minimum of 3 mice per genotype with ages ranging between P17 and P48 on a mixed C57BL6/129sv background. Bars, 200 μm (G to K) and 100 μm (L to N).

marked contrast to the lung, no *Pdgfa*$_{long}$ mRNA was detected in the central nervous system, which is in agreement with the observed normal spinal cord development in the various P*dgfa*$^{\Delta ex6}$ mutants analyzed.

Interpretation of the phenotypic consequences of the *Pdgfa*$^{\Delta ex6}$ allele are complicated by the fact that the *Pdgfa*$^{\Delta ex6}$ allele appears to be expression hypomorphic in some (lung and skin) but not other (e.g., intestine) organs, leading to a variable reduction in total PDGF-A transcript levels. It therefore remains to be elucidated if the lung phenotype observed in *Pdgfa*$^{\Delta ex6/-}$; *Pdgfr*α$^{+/+}$ and *Pdgfa*$^{\Delta ex6/-}$; *Pdgfr*α$^{GFP/+}$ mice is caused by the specific loss of PDGF-A$_{long}$, by reduced overall PDGF-A expression and signaling via PDGFRα to a level below a critical threshold, or by a combination of the two. The same problem exists for the developing vertebral column, which appears to be highly sensitive to the *Pdgfa* gene dose and for which we lack information on potential hypo-

morphic expression of the $Pdgfa^{\Delta ex6}$ allele. Nonetheless, our data suggest that expression hypomorphism of $Pdgfa^{\Delta ex6}$ is not general for all tissues and organs and may not explain all phenotypes observed in $Pdgfa^{\Delta ex6}$ mutants, such as in the intestine. This organ had the highest relative abundance of $Pdgfa_{long}$ mRNA ($Pdgfa_{long}$/$Pdgfa_{short}$ ratio, 1:1), showed a strong phenotype in $Pdgfa^{\Delta ex6/\Delta ex6}$; $Pdgfc^{-/-}$ mutants, and did not show signs of *Pdgfa* expression hypomorphism.

Alternative splicing of the PDGF-A gene is evolutionarily conserved. In *Xenopus*, PDGF-A signaling through PDGFRα has been implicated in the migration of embryonic mesoderm (49). In this system, PDGF-AA was recently shown to bind directly to HSPG-modified fibronectin, with a suggested role during cell migration and survival in *Xenopus* gastrulation (50). Our present genetic analysis of the $Pdgfa^{\Delta ex6}$ allele may suggest a role for PDGF-A_{long} in processes where the migration, proliferation, and/or survival of specific subsets of mesenchymal cells are implicated. These processes include the formation of the mesenchymal cell clusters implicated in intestinal villus formation (38), the formation of the dorsal arches of vertebrae (42, 43), and possibly the peripheral spreading and subsequent survival of alveolar smooth muscle cells during lung development (34). The precise functions of PDGF-A_{long} in these processes remain to be elucidated, but it is likely that the generation of local concentrations and possibly gradients of PDGF-A protein in the tissue plays a role, as previously suggested for VEGF-A (1, 2, 13) and PDGF-B (14, 15, 51).

In conclusion, we present an analysis of tissue-specific splicing of the *Pdgfa* mRNA during organ formation in the mouse, as well as the generation and analysis of mice selectively devoid of the long splice isoform of PDGF-A, PDGF-A_{long}. Our work suggests a subtle, but likely specific, role for the long splice isoform of PDGF-A in the intestine, and possibly also in other organs—a role that is partially redundant with those of PDGF-A_{short} and PDGF-C in an organ-specific manner. Our data also show that the same targeted mutation intended to block only splicing affected mRNA levels differently in different organs, thereby revealing an unforeseen caveat in the interpretation of phenotypic consequences of targeted mutagenesis in mice.

ACKNOWLEDGMENTS

We thank Silvia Bianconi for initial help with the generation of $Pdgfa^{\Delta ex6/\Delta ex6}$ mice and Sara Kamph, Helene Leksell, and Cecilia Olsson for technical assistance.

This work was supported by grants from the Ludwig Institute for Cancer Research; the Swedish Cancer Foundation; the Swedish Foundation for Strategic Research; the Novo Nordisk, Knut and Alice Wallenberg, IngaBritt and Arne Lundberg, Torsten and Ragnar Söderberg Foundation; and the Gothenburg Medical Society. H.D. is supported by CIHR and the Canada Research Chair Program.

REFERENCES

1. **Gerhardt H, Golding M, Fruttiger M, Ruhrberg C, Lundkvist A, Abramsson A, Jeltsch M, Mitchell C, Alitalo K, Shima D, Betsholtz C.** 2003. VEGF guides angiogenic sprouting utilizing endothelial tip cell filopodia. J. Cell Biol. **161:**1163–1177.
2. **Ruhrberg C, Gerhardt H, Golding M, Watson R, Ioannidou S, Fujisawa H, Betsholtz C, Shima DT.** 2002. Spatially restricted patterning cues provided by heparin-binding VEGF-A control blood vessel branching morphogenesis. Genes Dev. **16:**2684–2698.
3. **Rogers KW, Schier AF.** 2011. Morphogen gradients: from generation to interpretation. Annu. Rev. Cell Dev. Biol. **27:**377–407.
4. **Lindahl U, Li JP.** 2009. Interactions between heparan sulfate and proteins—design and functional implications. Int. Rev. Cell Mol. Biol. **276:**105–159.
5. **Ohkawara B, Iemura S, ten Dijke P, Ueno N.** 2002. Action range of BMP is defined by its N-terminal basic amino acid core. Curr. Biol. **12:**205–209.
6. **Häcker U, Nybakken K, Perrimon N.** 2005. Heparan sulphate proteoglycans: the sweet side of development. Nat. Rev. Mol. Cell Biol. **6:**530–541.
7. **Lin X.** 2004. Functions of heparan sulfate proteoglycans in cell signaling during development. Development **131:**6009–6021.
8. **Andrae J, Gallini R, Betsholtz C.** 2008. Role of platelet-derived growth factors in physiology and medicine. Genes Dev. **22:**1276–1312.
9. **Eriksson U, Alitalo K.** 1999. Structure, expression and receptor-binding properties of novel vascular endothelial growth factors. Curr. Top. Microbiol. Immunol. **237:**41–57.
10. **Ferrara N.** 2010. Binding to the extracellular matrix and proteolytic processing: two key mechanisms regulating vascular endothelial growth factor action. Mol. Biol. Cell **21:**687–690.
11. **LaRochelle WJ, May-Siroff M, Robbins KC, Aaronson SA.** 1991. A novel mechanism regulating growth factor association with the cell surface: identification of a PDGF retention domain. Genes Dev. **5:**1191–1199.
12. **Ostman A, Andersson M, Betsholtz C, Westermark B, Heldin CH.** 1991. Identification of a cell retention signal in the B-chain of platelet-derived growth factor and in the long splice version of the A-chain. Cell Regul. **2:**503–512.
13. **Carmeliet P, Ng YS, Nuyens D, Theilmeier G, Brusselmans K, Cornelissen I, Ehler E, Kakkar VV, Stalmans I, Mattot V, Perriard JC, Dewerchin M, Flameng W, Nagy A, Lupu F, Moons L, Collen D, D'Amore PA, Shima DT.** 1999. Impaired myocardial angiogenesis and ischemic cardiomyopathy in mice lacking the vascular endothelial growth factor isoforms VEGF164 and VEGF188. Nat. Med. **5:**495–502.
14. **Abramsson A, Kurup S, Busse M, Yamada S, Lindblom P, Schallmeiner E, Stenzel D, Sauvaget D, Ledin J, Ringvall M, Landegren U, Kjellén L, Bondjers G, Li JP, Lindahl U, Spillmann D, Betsholtz C, Gerhardt H.** 2007. Defective N-sulfation of heparan sulfate proteoglycans limits PDGF-BB binding and pericyte recruitment in vascular development. Genes Dev. **21:**316–331.
15. **Lindblom P, Gerhardt H, Liebner S, Abramsson A, Enge M, Hellström M, Backstrom G, Fredriksson S, Landegren U, Nyström HC, Bergström G, Dejana E, Ostman A, Lindahl P, Betsholtz C.** 2003. Endothelial PDGF-B retention is required for proper investment of pericytes in the microvessel wall. Genes Dev. **17:**1835–1840.
16. **Bonthron DT, Morton CC, Orkin SH, Collins T.** 1988. Platelet-derived growth factor A chain: gene structure, chromosomal location, and basis for alternative mRNA splicing. Proc. Natl. Acad. Sci. U. S. A. **85:**1492–1496.
17. **Rorsman F, Bywater M, Knott TJ, Scott J, Betsholtz C.** 1988. Structural characterization of the human platelet-derived growth factor A-chain cDNA and gene: alternative exon usage predicts two different precursor proteins. Mol. Cell. Biol. **8:**571–577.
18. **Betsholtz C, Johnsson A, Heldin CH, Westermark B, Lind P, Urdea MS, Eddy R, Shows TB, Philpott K, Mellor AL.** 1986. cDNA sequence and chromosomal localization of human platelet-derived growth factor A-chain and its expression in tumour cell lines. Nature **320:**695–699.
19. **Andersson M, Ostman A, Westermark B, Heldin CH.** 1994. Characterization of the retention motif in the C-terminal part of the long splice form of platelet-derived growth factor A-chain. J. Biol. Chem. **269:**926–930.
20. **Raines EW, Ross R.** 1992. Compartmentalization of PDGF on extracellular binding sites dependent on exon-6-encoded sequences. J. Cell Biol. **116:**533–543.
21. **Hoch RV, Soriano P.** 2003. Roles of PDGF in animal development. Development **130:**4769–4784.
22. **Matoskova B, Rorsman F, Svensson V, Betsholtz C.** 1989. Alternative splicing of the platelet-derived growth factor A-chain transcript occurs in normal as well as tumor cells and is conserved among mammalian species. Mol. Cell. Biol. **9:**3148–3150.
23. **Mercola M, Melton DA, Stiles CD.** 1988. Platelet-derived growth factor A chain is maternally encoded in Xenopus embryos. Science **241:**1223–1225.
24. **Collins T, Bonthron DT, Orkin SH.** 1987. Alternative RNA splicing affects function of encoded platelet-derived growth factor A chain. Nature **328:**621–624.
25. **Lustig F, Hoebeke J, Ostergren-Lundén G, Velge-Roussel F, Bondjers G, Olsson U, Rüetschi U, Fager G.** 1996. Alternative splicing determines the

binding of platelet-derived growth factor (PDGF-AA) to glycosaminoglycans. Biochemistry **35:**12077–12085.
26. **Lustig F, Hoebeke J, Simonson C, Ostergren-Lundén G, Bondjers G, Rüetchi U, Fager G.** 1999. Processing of PDGF gene products determines interactions with glycosaminoglycans. J. Mol. Recognit. **12:**112–120.
27. **Feyzi E, Lustig F, Fager G, Spillmann D, Lindahl U, Salmivirta M.** 1997. Characterization of heparin and heparan sulfate domains binding to the long splice variant of platelet-derived growth factor A chain. J. Biol. Chem. **272:**5518–5524.
28. **Ostman A, Bäckström G, Fong N, Betsholtz C, Wernstedt C, Hellman U, Westermark B, Valenzuela P, Heldin CH.** 1989. Expression of three recombinant homodimeric isoforms of PDGF in Saccharomyces cerevisiae: evidence for difference in receptor binding and functional activities. Growth Factors **1:**271–281.
29. **Eblen ST.** 2012. Regulation of chemoresistance via alternative messenger RNA splicing. Biochem. Pharmacol. **83:**1063–1072.
30. **Warzecha CC, Sato TK, Nabet B, Hogenesch JB, Carstens RP.** 2009. ESRP1 and ESRP2 are epithelial cell-type-specific regulators of FGFR2 splicing. Mol. Cell **33:**591–601.
31. **Grosso AR, Gomes AQ, Barbosa-Morais NL, Caldeira S, Thorne NP, Grech G, von Lindern M, Carmo-Fonseca M.** 2008. Tissue-specific splicing factor gene expression signatures. Nucleic Acids Res. **36:**4823–4832.
32. **Boström H, Willetts K, Pekny M, Levéen P, Lindahl P, Hedstrand H, Pekna M, Hellström M, Gebre-Medhin S, Schalling M, Nilsson M, Kurland S, Törnell J, Heath JK, Betsholtz C.** 1996. PDGF-A signaling is a critical event in lung alveolar myofibroblast development and alveogenesis. Cell **85:**863–873.
33. **Hamilton TG, Klinghoffer RA, Corrin PD, Soriano P.** 2003. Evolutionary divergence of platelet-derived growth factor alpha receptor signaling mechanisms. Mol. Cell. Biol. **23:**4013–4025.
34. **Lindahl P, Karlsson L, Hellström M, Gebre-Medhin S, Willetts K, Heath JK, Betsholtz C.** 1997. Alveogenesis failure in PDGF-A-deficient mice is coupled to lack of distal spreading of alveolar smooth muscle cell progenitors during lung development. Development **124:**3943–3953.
35. **Garcia P, Berlanga O, Watson R, Frampton J.** 2005. Generation of a conditional allele of the B-myb gene. Genesis **43:**189–195.
36. **Rucker EB, III, Dierisseau P, Wagner K-U, Garrett L, Wynshaw-Boris A, Flaws JA, Henninghausen L.** 2000. Bcl-X and Bax regulate mouse primordial germ cell survival and apoptosis during embryogenesis. Mol. Endocrinol. **14:**1038–1052.
37. **Fruttiger M, Karlsson L, Hall AC, Abramsson A, Calver AR, Boström H, Willetts K, Bertold CH, Heath JK, Betsholtz C, Richardson WD.** 1999. Defective oligodendrocyte development and severe hypomyelination in PDGF-A knockout mice. Development **126:**457–467.
38. **Karlsson L, Lindahl P, Heath JK, Betsholtz C.** 2000. Abnormal gastrointestinal development in PDGF-A and PDGFR-(alpha) deficient mice implicates a novel mesenchymal structure with putative instructive properties in villus morphogenesis. Development **127:**3457–3466.
39. **Calver AR, Hall AC, Yu WP, Walsh FS, Heath JK, Betsholtz C, Richardson WD.** 1998. Oligodendrocyte population dynamics and the role of PDGF in vivo. Neuron **20:**869–882.
40. **van Heyningen P, Calver AR, Richardson WD.** 2001. Control of progenitor cell number by mitogen supply and demand. Curr. Biol. **11:**232–241.
41. **Boström H, Gritli-Linde A, Betsholtz C.** 2002. PDGF-A/PDGF alpha-receptor signaling is required for lung growth and the formation of alveoli but not for early lung branching morphogenesis. Dev. Dyn. **223:**155–162.
42. **Ding H, Wu X, Boström H, Kim I, Wong N, Tsoi B, O'Rourke M, Koh GY, Soriano P, Betsholtz C, Hart TC, Marazita ML, Field LL, Tam PP, Nagy A.** 2004. A specific requirement for PDGF-C in palate formation and PDGFR-alpha signaling. Nat. Genet. **36:**1111–1116.
43. **Soriano P.** 1997. The PDGF alpha receptor is required for neural crest cell development and for normal patterning of the somites. Development **124:**2691–2700.
44. **Ding H, Wu X, Kim I, Tam PP, Koh GY, Nagy A.** 2000. The mouse Pdgfc gene: dynamic expression in embryonic tissues during organogenesis. Mech. Dev. **96:**209–213.
45. **Karlsson L, Bondjers C, Betsholtz C.** 1999. Roles for PDGF-A and sonic hedgehog in development of mesenchymal components of the hair follicle. Development **126:**2611–2621.
46. **Gnessi L, Basciani S, Mariani S, Arizzi M, Spera G, Wang C, Bondjers C, Karlsson L, Betsholtz C.** 2000. Leydig cell loss and spermatogenic arrest in platelet-derived growth factor (PDGF)-A-deficient mice. J. Cell Biol. **149:**1019–1026.
47. **Afrakhte M, Nistér M, Ostman A, Westermark B, Paulsson Y.** 1996. Production of cell-associated PDGF-AA by a human sarcoma cell line: evidence for a latent autocrine effect. Int. J. Cancer **68:**802–809.
48. **Li SH, Lee RK, Chen PW, Lu CH, Wang SH, Hwu YM.** 2005. Differential expression and distribution of alternatively spliced transcripts of PDGF-A and of PDGF receptor-alpha in mouse reproductive tissues. Life Sci. **77:**2412–2424.
49. **Symes K, Mercola M.** 1996. Embryonic mesoderm cells spread in response to platelet-derived growth factor and signaling by phosphatidylinositol 3-kinase. Proc. Natl. Acad. Sci. U. S. A. **93:**9641–9644.
50. **Smith EM, Mitsi M, Nugent MA, Symes K.** 2009. PDGF-A interactions with fibronectin reveal a critical role for heparan sulfate in directed cell migration during Xenopus gastrulation. Proc. Natl. Acad. Sci. U. S. A. **106:**21683–21688.
51. **Abramsson A, Lindblom P, Betsholtz C.** 2003. Endothelial and nonendothelial sources of PDGF-B regulate pericyte recruitment and influence vascular pattern formation in tumors. J. Clin. Invest. **112:**1142–1151.